Topology Optimization for the Design of a Heat Sink in an Inductive Electrically Excited Synchronous Machine

Simon Knecht* and Albert Albers†

Institute of Product Engineering, Karlsruhe Institute of Technology, Karlsruhe, 76131, Germany

Andreas Baehr* and Nejila Parspour†

Institute of Electrical Energy Conversion, University of Stuttgart, Stuttgart, 70569, Germany

Holger Ahlborn* and Peter Middendorf†

Institute of Aircraft Design, University of Stuttgart, Stuttgart, 70569, Germany

An inductive electrically excited synchronous machine does not require permanent magnets or slip rings. It is therefore beneficial concerning its supply chain and has less wear. Compared to a permanent magnet synchronous machine, the wireless power transfer system introduces additional complexity. The heat generated by losses in the coils and rectifier of the wireless power transfer system must be taken out of the system by active cooling. In this work, we show how we used the method of topology optimization to create a design for the rectifier heat sink. The optimized heat sink makes use of its rotation to efficiently cool the rectifier diodes. In order to manufacture the heat sink, a manual redesign was necessary which altered the optimized design. Future work will look into manufacturing methods to better capture the design features of the optimized design.

I. Introduction

In a previous research project, a highly integrated wireless power transfer (WPT) system was developed for the use in an inductive electrically excited synchronous machine (iEESM).[1] An electrically excited synchronous machine (EESM) has the advantage that it does not require permanent magnets and has a higher efficiency over a wide range of operating points compared to a permanent magnet synchronous machine.[3] In an iEESM, the slip rings of an EESM are replaced by a wireless power transfer (WPT) system for energy transfer by inductive energy transfer through coupled coils to reduce friction and wear. The proposed design integrates both the coils as well as the passive rectifier in a hollow shaft made from glass fiber reinforced plastic (fig. 1). This reduces the required installation space compared to an axially mounted WPT system[4] while at the same time saving weight.

This WPT system is able to transfer up to 2.5 kW of electrical power to the rotor. This results in power losses not only in the coils but also in the rectifier diodes. In order to effectively transport the heat from the diodes to the cooling air flow, a sophisticated heat sink had to be designed. In this paper, we present how we used the method of topology optimization to create a design proposal for this heat sink.

II. Model setup

Since the coils are downstream of the heat sink, they are assumed to have a negligible effect on the heat sink design, taking into account the given boundary conditions and optimization constraints, and were therefore not included in the simulation model.

All simulations and optimizations were carried out in Siemens Simcenter Star-CCM+ 2302 Build 18.02.008. The underlying model of the geometry representation during the optimization is the level-set method. In this method, a variable Φ serves as the representation of solid and fluid phase in the optimization domain. Φ varies between -1 and 1 which corresponds to the solid and fluid phase, respectively.

*Scientific Researcher

†Head of Institute

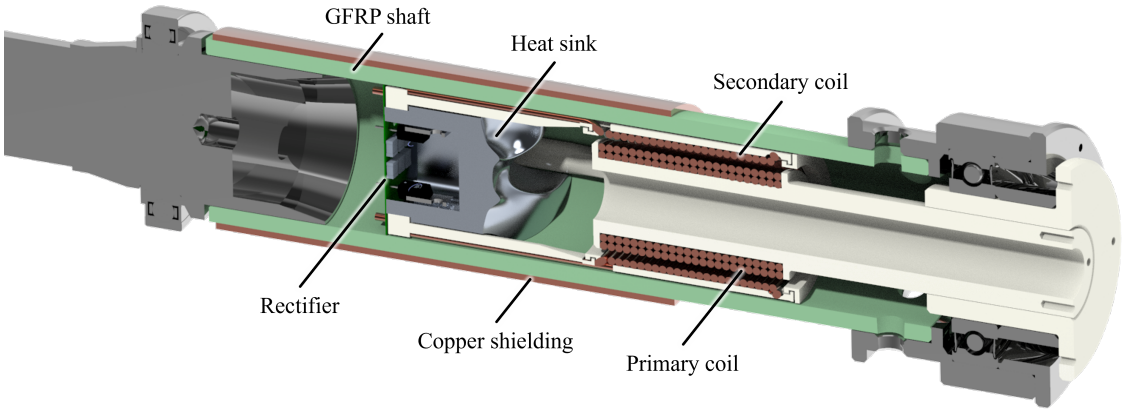

Figure 1. Cut view through the final design iteration of the hollow shaft with integrated wireless power transfer system

A value of $\Phi = 0$ implicitly describes the interface between solid and fluid phase. The distribution is varied in time by the following equation:

$$\frac{\partial \Phi}{\partial \tau} + F||\nabla \Phi|| = S \tag{1}$$

where τ is a pseudo time, F is the interface velocity and S is the source term. This source term is omitted in all optimizations (see sec. II.A). The level-set equation is translated to a material distribution by the following equation:

$$\mathcal{X} = 0.5 \cdot \left(1 + tanh\left(\frac{\Phi}{0.056}\right)\right) \tag{2}$$

where $\mathcal{X}$ is the material distribution ranging from 0 (solid) to 1 (fluid).

The effect of the solid material on the flow field is modelled by the Brinkman Penalization.[2] This penalization introduces an additional term to the momentum equation:

$$\frac{\partial \mathbf{v}}{\partial t} + \nabla \cdot (\rho \mathbf{v} \otimes \mathbf{v}) = -\nabla \cdot \sigma \underbrace{-\alpha(1-\mathcal{X})\mathbf{v}}_{\text{Brinkman Penalization}} \tag{3}$$

where ρ is the density, $\mathbf{v}$ the velocity, σ the stress tensor and α the Brinkman Penalization magnitude, which was set to $\alpha = 1\text{e}7$.

II.A. Two-dimensional setup

To start with the optimization, two-dimensional simulation models were set up to investigate different optimization parameters. The computational cost was relatively low compared to the following three-dimensional simulation models. This allowed for quick iterations on different parameter values and combinations. With this setup, the most relevant optimization parameters could be identified.

The two-dimensional model consists of the cooling airflow and the base of the heat sink. The optimization domain was placed between the heat sink's base and the airflow. The base of the heat sink serves as a fixed solid volume to introduce heat into the system. Rotation was neglected in the two-dimensional simulation model. A schematic and the dimensions of the simulation setup are given in fig. 2.

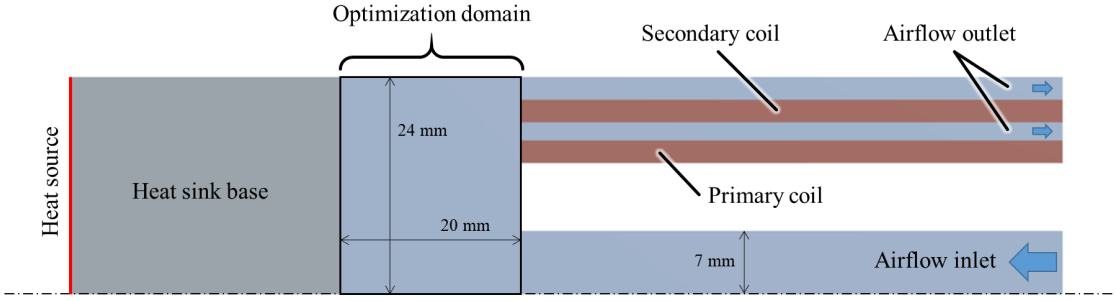

Figure 2. Setup of the two-dimensional simulation model

The parameters that were investigated include the formulation of the objective function, constraints for the optimization, the initial material distribution, and hole formation (corresponds in this case to blobs of solid forming).

For the objective function, two different variants were investigated: Maximizing the heat transfer between heat sink base and optimization domain with a given temperature and minimizing the temperature of the heat sink base with a given heat source. Both options produced good results. For the two-dimensional optimization runs, the heat transfer was maximized for a given prescribed temperature.

The different constraints investigated were a volume constraint on the solid region and a pressure loss constraint. The volume constraint was chosen arbitrarily to ensure a predefined mass of the heat sink. The pressure loss constraint was necessary in order to receive feasible optimization results (see fig. 3 c)).

The initial material distribution was varied between separate blobs and a negative half-circle (see fig. 3 a) and b)). The separate blobs created promising results regarding the heat transfer and flow pattern, but these results often had floating parts separated from the heat sink body so they cannot be manufactured. An initial material distribution consisting of a negative half-circle provided less intricate geometries, but the results consisted of a single coherent heat sink.

The last parameter that was investigated was the hole formation within the optimization domain. This option introduces a source term into the level-set function which corresponds to pockets of solid forming in the optimization domain (see eq. 1). As with the initial material distribution of separate blobs, these pockets of solid introduced many free floating parts (see fig. 3 d)). The hole formation was therefore turned off for all subsequent optimization runs.

Figure 3 shows initial material distributions and different optimization results. It can clearly be seen in fig. 3 c), that without a constraint on the pressure loss, the resulting heat sink is physically not feasible. The Brinkman penalization as introduced in eq. 3 forces the velocity in the solid phase towards zero, but not exactly zero. Therefore there is still a flow creeping through the solid phase. This flow creates a very large pressure drop of 4.22e5 Pa in this case.

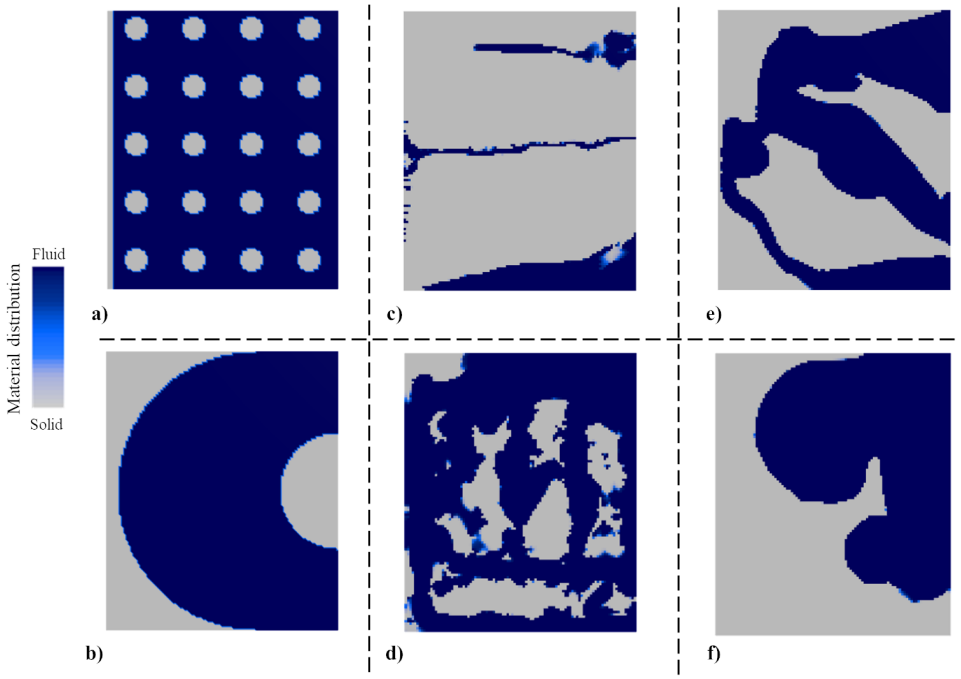

Figure 3. Initial material distributions and results of two-dimensional optimizations. a) Initial distribution consisting of small pockets of solid. b) Initial distribution consisting of a negative half-circle. c) Result without a constraint on the pressure drop. d) Result with hole formation allowed. e) Result with pressure drop constraint and without hole formation from initial distribution a). f) Result with pressure drop constraint and without hole formation from initial distribution b).

From the two-dimensional results we concluded, that in this case a constraint on the pressure drop is necessary while the hole formation should be turned off to get feasible results as can be seen in fig. 3 f).

II.B. Three-dimensional setup

The three-dimensional simulation model was set up in a similar way as the two-dimensional model. The geometry near the inlet and outlet was slightly altered due to a new design iteration. A quarter section of the whole system was modelled to reduce the computational cost and to ensure rotational symmetry of

the resulting heat sink geometry. The simulation model includes an axial groove to guide the wires from the coils to the rectifier and back. The flow was driven by a pressure difference of 0.1 bar between inlet and outlet. This pressure-driven flow made an additional constraint on the pressure drop redundant. The rotation was modelled using a steady-state moving reference frame. Figure 4 shows the setup of the three-dimensional simulation model.

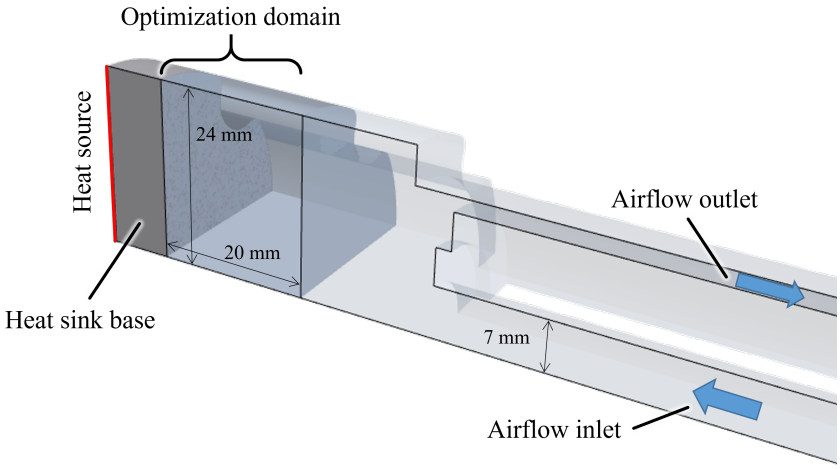

Figure 4. Setup of the three-dimensional simulation model

The electromagnetic simulation predicted a heat loss of 40 W in the rectifier. This heat loss was introduced at the back side of the heat sink base. Therefore the objective function was chosen to minimize the average heat sink temperature with the given heat loss. A turned negative half-circle was chosen for the initial material distribution as it provided the best results in the two-dimensional optimization runs.

III. Optimization Result

The three-dimensional optimization was run for 300 iterations. The total computational time was approximately 9 hours.

The optimization result is shown in fig. 5. The geometry shown is created by an isosurface at $\mathcal{X} = 0.5$. The structure consists of four claw-like shapes with a rough surface. One reason for the roughness could be the derivation of the isosurface in combination with the volumetric discretization by polyhedra. Another possibility could be the that the surface is deliberately generated to increase the heat transfer. The material distribution shows a sharp interface which is beneficial for the derivation of an optimized geometry.

The optimization result was supposed to be validated by experimental measurements. It was chosen to manufacture the heat sink by milling. Since the optimization result features detailed geometries and a rough surface, manufacturing costs by milling would be very high. We therefore did a manual redesign of the resulting geometry.

Figure 6 shows the process of the redesign. On the left hand, a cleaned-up version of the original optimization result is shown. We removed free-floating pockets of solid and delicate structures that would easily break. The most prominent features of the remaining surface were then manually remodelled by polygonal patches. After smoothing the polygonal patches, the final heat sink design was achieved.

IV. Experimental validation

To ensure the validity of the simulation model from sec. II.B, an experimental validation of the WPT system was carried out. The measurements were taken in a non-rotating system, since the rotating subsystem and high-power WPT system introduce a lot of complexity into the system. The corresponding simulation model was adjusted to reproduce the experimental setup. The optimized heat sink geometry was replaced by the smoothed redesign. Figure 7 shows a diagram of a generic validation environment for an iEESM, its involved physical and virtual subsystems and their interrelations. We considered only a stationary WPT system without the rest of the electric machine. Therefore, the virtual machine model and the rotor model were omitted. In addition, no transfer of power or data between rotating and stationary system was needed which further reduced the complexity.

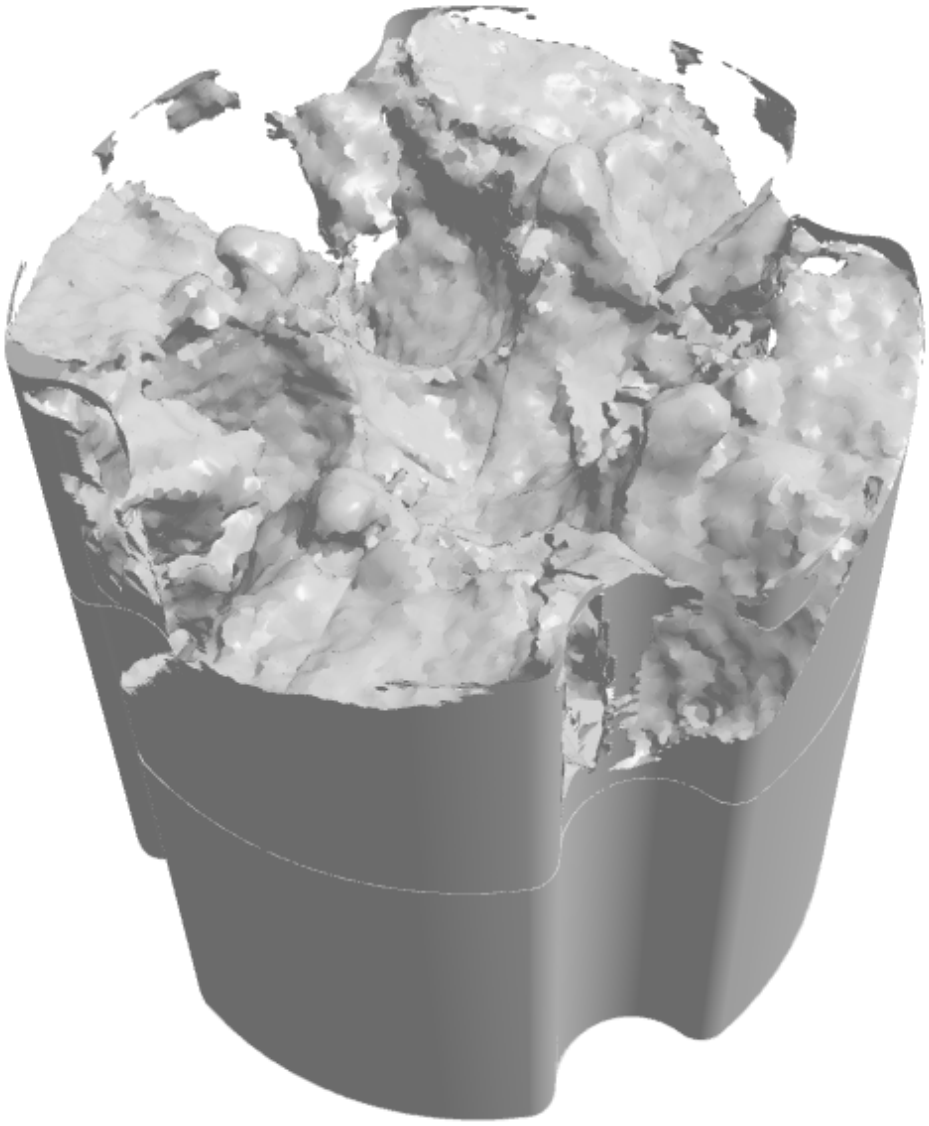

Figure 5. Optimization result of the three-dimensional optimization. Shown is an isosurface at $\mathcal{X} = 0.5$.

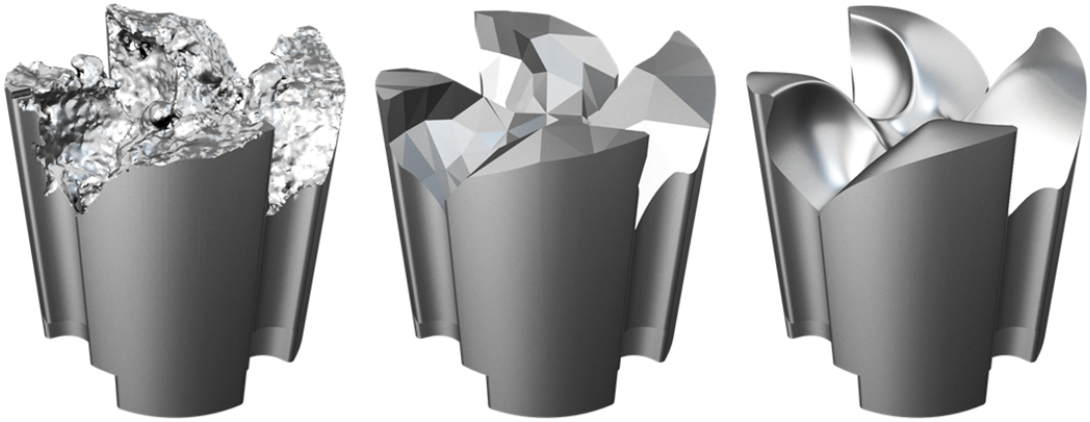

Figure 6. Redesign process: Cleaned-up optimization result (left), polygonal redesign (middle), smoothed surface ready for manufacturing (right)

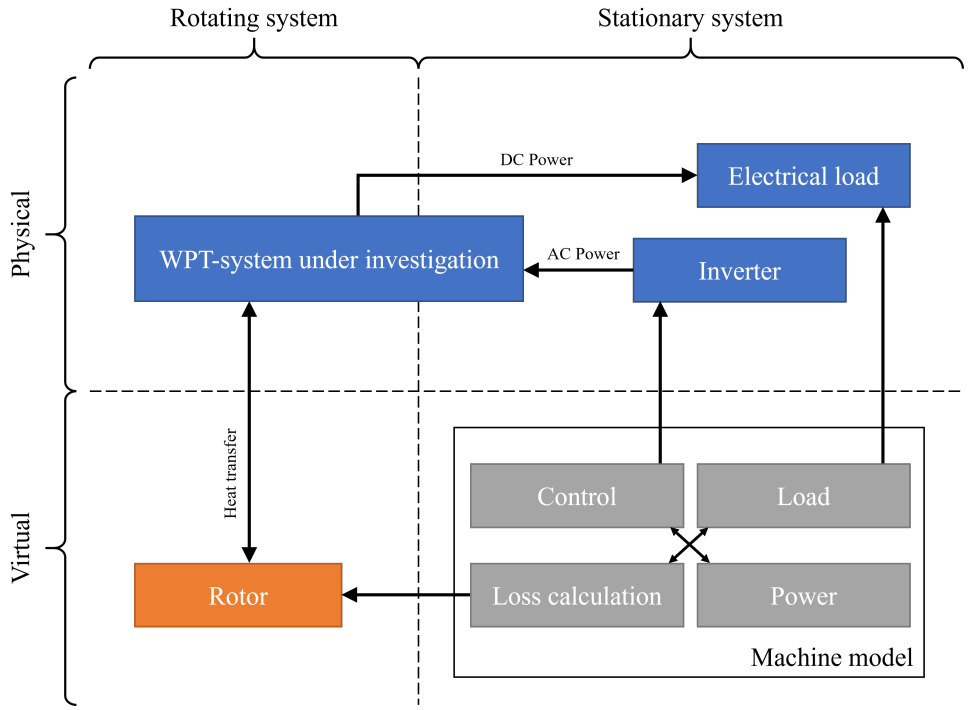

Figure 7. Diagram of a generic validation environment containing involved physical and virtual subsystems and their interrelations. Within this work, a stationary WPT system was investigated. Therefore, only inverter, non-rotating WPT system, load and measurement equipment were present.

IV.A. Setup

Figure 8 shows the experimental setup for the validation. The heat sink was manufactured from 6060 aluminium alloy and installed in the hollow shaft. Temperatures on the heat sink's outer surface and within the coils were measured through thermocouples. Since the high-frequency magnetic field interferes with the thermocouples, a continuous measurement during power transfer was not possible. Instead, the power transfer was paused at regular intervals to allow for a temperature measurement without interference. This procedure was repeated until constant temperatures were measured. This inevitably leads to small errors, as the temperatures start decreasing as soon as the power transfer is cut off. We assume however that the introduced errors are small enough to still enable an acceptable validation.

For the validation test run, a continuous power of 961.94 W was transferred over the WPT system. The DC/DC-efficiency reached 94.55 % which results in total losses of $P_{l,tot} = 52.38$ W. Of these losses, $P_{l,rect} \approx 17.16$ W come from the rectifier diodes and therefore need to be dissipated by the heat sink. The cooling airflow was regulated by a valve to a continuous airflow of $Q = 5$ m^3/h at a temperature of $T_{in} = 24.4\,°\mathrm{C}$. The throttling effect of the small-diameter pipe between flow rate measurement and WPT system had to be accounted for when calculating the effective flow rate through the WPT system. The simulation model was adapted accordingly.

Type J thermocouples were placed on the casings of both rectifier diodes and on two symmetrical locations of the heat sink. A piece of electrically isolating tape was placed between each thermocouple and its measurement location.

IV.B. Validation results

The temperature measurements on the rectifier diodes and on the heat sink were both within 1 K of each other, respectively. Therefore, we can rule out measurement errors introduced by irregular placement of the thermocouples. To compare the measurements with simulation results, the average of both thermocouples was taken.

Table 1. Comparison of temperature readings between simulation and experiment

Measurement location	Simulation [°C]	Experiment [°C]
Rectifier diode casing	83.8	88.5
Outer heat sink surface	56.5	60.4

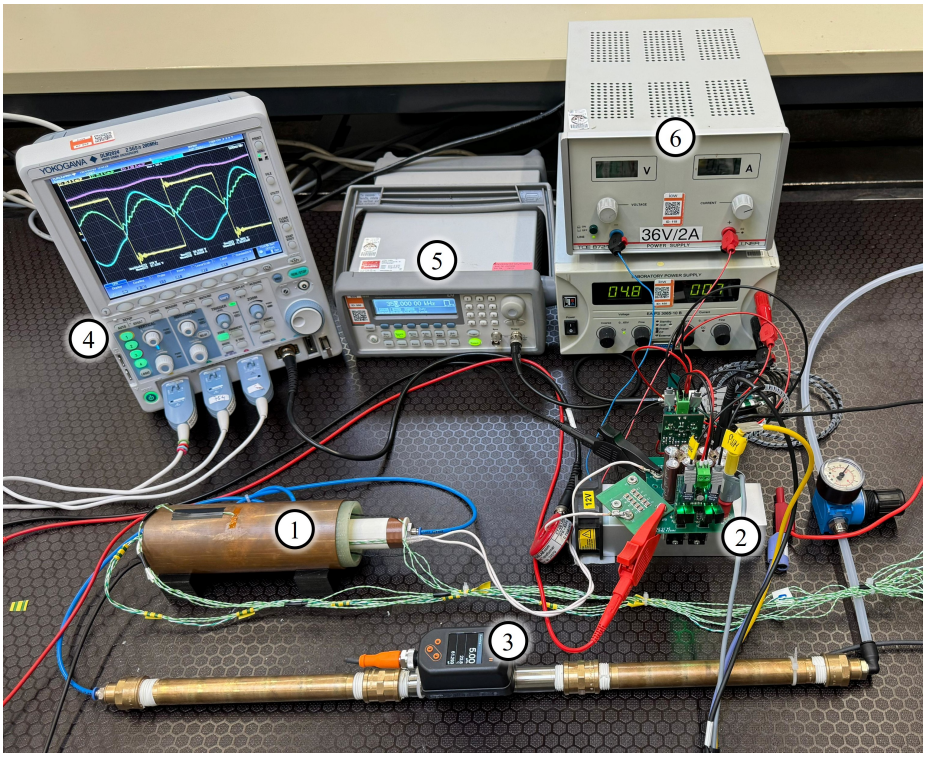

Figure 8. Experimental setup for the validation of the simulation model in the non-rotating system. 1) The WPT system under investigation. 2) Inverter of the WPT system. 3) Flow rate measurement. 4) Electronic measurements. 5) Frequency generator for the inverter. 6) Peripheral power supply. Not shown are the main power supply and the electrical load.

Table 1 shows a comparison between measured temperatures and temperatures taken from the simulation. A maximum temperature difference of 4.71 K shows a relatively good agreement between simulation and experiment. Overall, the simulation predicted slightly lower temperatures than the experiment. One possible reason for this could be a too high estimate of the heat dissipation through natural convection via the outer surface of the WPT system.

V. Conclusion & Outlook

In this work, we used the method of topology optimization to create a heat sink design for the use in an inductive electrically excited synchronous machine. We did preliminary investigations into the optimization and involved parameters by simplified two-dimensional models. A three-dimensional optimization was carried out on a quarter section. The initial design proposal was manually redesigned to enable manufacturing by milling. We manufactured the heat sink and did first experimental measurements to validate the underlying simulation model.

It became clear that the optimization strongly depends on the choice of input parameters such as the initial material distribution. Furthermore, the choice of a moving reference frame for modelling the rotation might not be suitable to capture the flow field resulting from the detailed heat sink geometries. The problem of structural integrity and manufacturability of the heat sink was tackled by manually redesigning the optimized heat sink.

In future works, we want to incorporate the mechanical aspect already in the optimization. This potentially enables the use of additive manufacturing for a heat sink with internal cooling channels. Through additive manufacturing, the complex optimized geometry can be more accurately manufactured. In addition, the rotation must be looked at to properly model its influence on the flow field. Furthermore, we want to extend the test bench for experimental validation to create measurements in the rotating system.

Acknowledgements

The authors would like to thank the Ministry of Science, Research and Arts of the Federal State of Baden-Württemberg for the financial support of this project within the InnovationCampus Future Mobility (ICM).

References

[1]Andreas Baehr, Holger Ahlborn, Simon Knecht, and Nejila Parspour. Highly Integrated Wireless Power Transfer System for an Inductive Electrically Excited Synchronous Machine. In *2024 IEEE Wireless Power Technology Conference and Expo (WPTCE)*, pages 64–68, Kyoto, Japan, May 2024. IEEE.

[2]Henry Coenraad Brinkman. A calculation of the viscous force exerted by a flowing fluid on a dense swarm of particles. *Flow, Turbulence and Combustion*, 1(1):27, December 1949.

[3]Georgios Mademlis, Yujing Liu, Junfei Tang, Luca Boscaglia, and Nimananda Sharma. Performance Evaluation of Electrically Excited Synchronous Machine compared to PMSM for High-Power Traction Drives. In *2020 International Conference on Electrical Machines (ICEM)*, pages 1793–1799, Gothenburg, Sweden, August 2020. IEEE.

[4]Samuel Müller, David Maier, and Nejila Parspour. Inductive Electrically Excited Synchronous Machine for Electrical Vehicles—Design, Optimization and Measurement. *Energies*, 16(4):1657, February 2023.